© 2016. Published by The Company of Biologists Ltd | Journal of Experimental Biology (2016) 219, 3339-3352 doi:10.1242/jeb.136820

RESEARCH ARTICLE

Object approach computation by a giant neuron and its relationship with the speed of escape in the crab *Neohelice*

Damián Oliva[1] and Daniel Tomsic[2,*]

ABSTRACT

Upon detection of an approaching object, the crab *Neohelice granulata* continuously regulates the direction and speed of escape according to ongoing visual information. These visuomotor transformations are thought to be largely accounted for by a small number of motion-sensitive giant neurons projecting from the lobula (third optic neuropil) towards the supraesophageal ganglion. One of these elements, the monostratified lobula giant neuron of type 2 (MLG2), proved to be highly sensitive to looming stimuli (a 2D representation of an object approach). By performing *in vivo* intracellular recordings, we assessed the response of the MLG2 neuron to a variety of looming stimuli representing objects of different sizes and velocities of approach. This allowed us to: (1) identify some of the physiological mechanisms involved in the regulation of the MLG2 activity and test a simplified biophysical model of its response to looming stimuli; (2) identify the stimulus optical parameters encoded by the MLG2 and formulate a phenomenological model able to predict the temporal course of the neural firing responses to all looming stimuli; and (3) incorporate the MLG2-encoded information of the stimulus (in terms of firing rate) into a mathematical model able to fit the speed of the escape run of the animal. The agreement between the model predictions and the actual escape speed measured on a treadmill for all tested stimuli strengthens our interpretation of the computations performed by the MLG2 and of the involvement of this neuron in the regulation of the animal's speed of run while escaping from objects approaching with constant speed.

KEY WORDS: Looming, Collision avoidance, Motion detection, Lobula neurons, Escape response, Crustacean

INTRODUCTION

Upon the sight of an approaching predator, an animal has to decide in a timely manner at what moment, in what direction and with what speed it should escape from the impending threat. To deal with these challenges, most visual animals possess movement-sensitive neurons in which the highest activity is recorded in response to objects approaching on a collision course (or their 2D representation, known as looming stimuli). Such neurons are commonly referred as looming sensitive neurons (LSNs). LSNs have been found in pigeons (Wang and Frost, 1992), fish (Preuss et al., 2006), monkeys (Maier et al., 2004) and different arthropod species such as locusts (Rind and Simmons, 1992; Gabbiani et al., 1999; Gray et al., 2010), flies (Borst, 1991; Fotowat et al., 2009), crayfish (Glantz, 1974) and crabs (Oliva et al., 2007; Oliva and Tomsic, 2014). But, how is the visual information of an approaching object actually processed, encoded and conveyed by LSNs to contribute to avoidance behaviors? This is a complex problem for which some insect and crustacean models have proved to offer considerable advantages (Herberholtz and Marquart, 2012).

The most compelling studies have been performed in the lobula giant movement detector (LGMD) neuron of the locust. These studies have shown that a number of biophysical mechanisms work in parallel to cast the visual response of the LGMD. These mechanisms comprise feed-forward excitation and feed-forward inhibition, adaptation, lateral inhibition and synchronization (reviewed in Fotowat and Gabbiani, 2011; Oliva, 2015). Another important conclusion from studies of the locust's response to looming stimuli is that the LGMD is important for the timely performance of the avoidance responses, but not entirely necessary for the behavioral execution of the escape (Santer et al., 2008; Simmons et al., 2010; Fotowat et al., 2011), indicating that additional LSN elements work in parallel to achieve the task (Rind, 1996; Gray et al., 2010).

Visually guided collision avoidance behaviors (VGCABs) differ noticeably according to the animal's locomotion mode and living environment (Oliva, 2015). Considering that the motor output is regulated by an input optical variable, these behaviors are usually phenomenologically described. Some VGCABs can be described as all-or-none responses initiated when an optical variable surpasses a certain threshold value. This category of VGCAB was found in the crayfish defensive reflex (Glantz, 1974) and in flies (Borst and Bahde, 1988; Tammero and Dickinson, 2002). Other VGCABs include multiple response components, each one being launched when an optical variable attains a specific threshold. This type of multistage responses was observed in locusts (e.g. Santer et al., 2005; Fotowat and Gabbiani, 2007; Fotowat et al., 2011), flies (Card and Dickinson, 2008; Fotowat et al., 2009) and crabs (Hemmi and Tomsic, 2012). Finally, other VGCABs are continuously regulated according to visual information changes in the position, direction and speed of the approaching object. Such behaviors have been investigated in connection with animal navigation (e.g. Srinivasan and Zhang, 2004), and less often in connection with predator avoidance (Land and Layne, 1995; Oliva and Tomsic, 2012; Medan et al., 2015).

One of the challenges when investigating the computational and neural processes that underlie VGCABs is the scarcity of experimental models in which both the behavioral and the neuronal responses can be studied in the same animal (Fotowat and Gabbiani, 2011). The avoidance escape behaviors that had been so far correlated with neuronal activity are of the all-or-none type or the multistage type, i.e. involving threshold response values.

Recently, we have shown that when escaping from a visual threat, the crab *Neohelice* adjusts the speed and the direction of run as a function of the visual changes generated by the moving stimulus.

[1]Departamento de Ciencia y Tecnología, Universidad Nacional de Quilmes, Quilmes (1878), CONICET, Argentina. [2]Departamento Fisiología, Biología Molecular y Celular, Facultad de Ciencias Exactas y Naturales, Universidad de Buenos Aires, IFIBYNE-CONICET, Pabellón 2 Ciudad Universitaria (1428), Buenos Aires, Argentina.

*Author for correspondence (tomsic@fbmc.fcen.uba.ar)

D.T., 0000-0002-2273-5927

Received 23 December 2015; Accepted 16 August 2016

Journal of Experimental Biology (2016) 219, 3339-3352 doi:10.1242/jeb.136820

Whereas the decision to initiate the escape depends on a threshold value (a particular increment of the stimulus angular size), the running itself does not constitute a ballistic type of response, as its speed is regulated according to the dynamic of stimulus expansion, and as the animal immediately decelerates at any time, the stimulus stops growing. We found that the speed of the escape run can be accurately described by a phenomenological input–output relationship built on the stimulus angular increment and the angular velocity of the stimulus (Oliva and Tomsic, 2012). We also showed that when escaping from a visual threat, the crab *Neohelice* continuously adjusts its running direction when the position of the visual threat changes by less than 1 deg (Medan et al., 2015). These results indicate that the speed and direction of the escape run are continually controlled by visually regulated mechanisms.

We have identified at least two different classes of LSNs from the lobula of the crab (Medan et al., 2007; Oliva et al., 2007) that are candidates to play a central role in the regulation of the visually guided escape behavior. One cell type is the monostratified lobula giant of type 1 (MLG1). There are 16 MLG1 neurons, whose receptive fields are uniformly allocated across the transversal axes of the lobula (the axes that contains the azimuthal representation of the visual space; Berón de Astrada et al., 2011). In conjunction, the ensemble of MLG1s covers the 360 deg visual field seen by each eye of the crab (Medan et al., 2007; Sztarker et al., 2005). MLG1s have been recently characterized in terms of their responses to looming stimuli and their possible role in the control of the direction and speed of escape (Medan et al., 2015), and their responses have been modeled (Oliva and Tomsic, 2014). Therefore, within this work we focused on the other cell type, the monostratified lobula giant of type 2 (MLG2), which is a much larger neuron than the MLG1s. The dendritic tree of MLG2 extends over the entire retinotopic mosaic of the lobula, thus collecting information from the entire visual field. There is apparently only one MLG2 per lobula (Medan et al., 2007; Sztarker et al., 2005). In order to compare the performance of the MLG2 neuron with the previously investigated performance of MLG1 neurons of the crab, in this study we applied the same methodology that we employed in our previous study on the MLG1 neurons (Oliva and Tomsic, 2014).

Using a variety of looming stimuli representing objects of different sizes approaching at different constant velocities, here we characterized the response of the MLG2 neuron, identified the main parameters that shape its response, and adapted a biophysical model to capture the relevant physiological mechanisms that regulate the encoding of looming stimuli. We also found that the firing rate of MLG2 encode information on the stimulus angular velocity. Because our phenomenological model (Oliva and Tomsic, 2012) indicates that angular velocity is one of the two stimulus optical parameters that seem to be used by the crab to regulate its speed of escape, we tested the reliability of the information conveyed by MLG2 during the looming-elicited escape response by replacing the stimulus angular velocity of the model with the neuronal firing rate. The results show a good agreement between the model predictions and the actual escape speed measured for all tested stimuli.

MATERIALS AND METHODS

Animals

Animals were adult male *Neohelice granulata* (Dana 1851) crabs 2.7–3.0 cm across the carapace, weighing approximately 17 g, collected in the rías (narrow coastal inlets) of San Clemente del Tuyú, Argentina. The crabs were maintained in plastic tanks filled to 2 cm depth with artificial seawater prepared using hw-Marinex (Winex, Hamburg, Germany), salinity 10–14‰, at a pH of 7.4–7.6. The holding and experimental rooms were maintained within a range of 22–24°C and were kept on a 12 h:12 h light:dark cycle (lights on 07:00 to 19:00 h), and the experiments were run between 08:00 and 19:00 h at room temperature.

Visual stimuli

Computer-generated visual stimuli were projected alternatively on three flat-screen monitors (Phillips 107T; horizontal and vertical screen dimensions were 32 and 24 cm respectively, refreshing rate 60 Hz). In behavioral and electrophysiological experiments, the crab was positioned in the center of the arrangement of these monitors, located 20 cm in front of and on both sides of the animal (Fig. 1). The monitors were covered with anti-glare screens to reduce reflections between them. All visual stimuli were generated with a PC using commercial software (Presentation 5.3, Neurobehavioral Systems, Albany, CA, USA). Except for the results shown in Fig. 2, all the experiments of the present study were performed with stimuli presented only on the monitor located to the right of the animal. This was chosen because crabs run sideways and keep the image of fast-moving stimuli at a fixed position on the lateral pole, where they have the highest visual acuity (Land and Layne, 1995; Medan et al., 2015). Although the crab's monocular visual field encompasses 360 deg, the visual area oriented toward the middle of the crab (i.e. looking to the contralateral side) has poorer acuity (Berón de Astrada et al., 2012).

Visual simulations generated by a computer may differ in many ways from the visual input experienced under natural conditions. For example, the refresh rate of a monitor screen may impose a severe constraint on the study of the visual system of animals with a high flicker fusion frequency. Flicker fusion in the fiddler crab *Uca pugilator* was found to be below 50 Hz (Layne et al., 1997). We did not measure the fusion frequency in *Neohelice*, but are confident that it is lower than the refresh rate of our monitors. In fact, we found no differences between the escape response elicited by a black sheet of cardboard approaching the animal and the computer simulation of an object of the same size and speed of approach (D. Oliva, Mechanisms of visual detection and avoidance of collision stimuli in a new experimental model, the crab *Chasmagnathus granulatus*, PhD thesis, University of Buenos Aires, 2010).

Looming stimuli

Looming stimuli simulated dark square objects of various sizes approaching with constant velocities on a direct collision course towards the animal (Fig. 1A). Black squares expanded on a white background, being the irradiance of the black square 4 mW m^{-2} and that of the white background 240 mW m^{-2}, measured at the monitor screen level. Let l denote the object half-size. The distance between the animal eye and the virtual object at time t is $x(t)$, and the object subtends an angle $\theta(t)$ on the eye. Thus, we can write:

$$\tan[\theta(t)/2] = \frac{l}{x(t)}, \quad (1)$$

with the chosen coordinate system and time definitions, we have $x(t) \geq 0$, $t \geq 0$. Objects were simulated to start their approach from a distance of L=5 m. The position of the object is given by:

$$x(t) = L - v \cdot t, \quad (2)$$

Journal of Experimental Biology (2016) 219, 3339-3352 doi:10.1242/jeb.136820

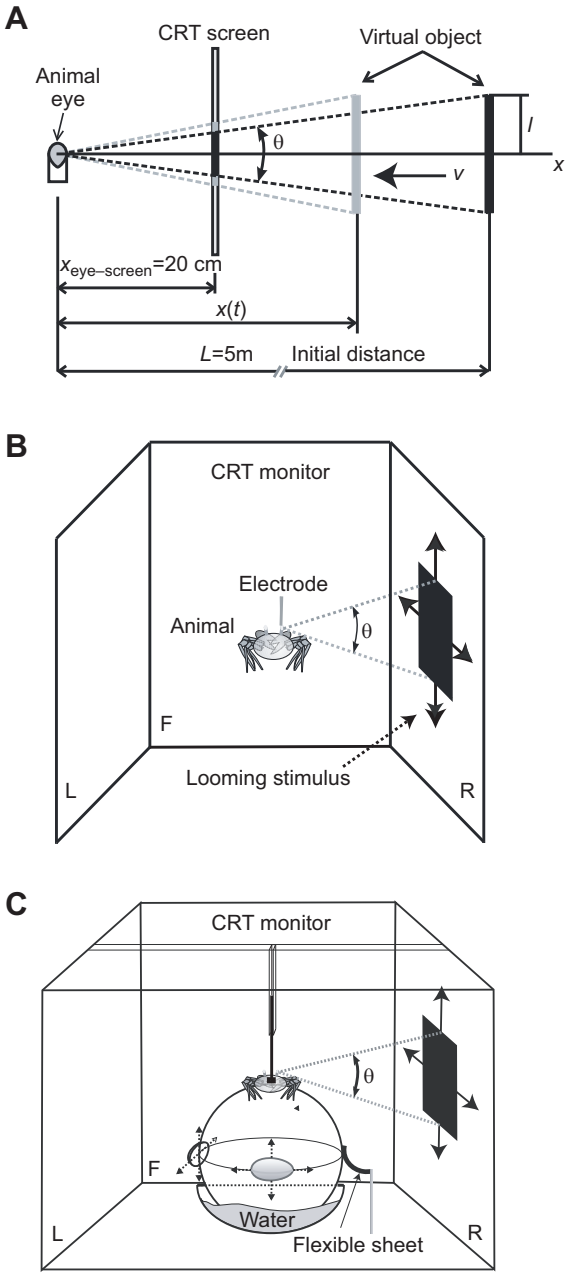

Fig. 1. Looming stimuli generation, electrophysiology and behavior. (A) Simulation of an object approaching at constant velocity shown at two different times. $x(t)$ is the distance of the object in a reference system centered on the crab, v is the velocity of approach towards the crab (horizontal arrow), θ is the total angle subtended by the object at the eye of the crab and l is the half-size of the object. (B) Electrophysiological measurements. Computer-generated visual stimuli were projected alternatively on three flat-screen CRT monitors located 20 cm in front of and on both sides of the animal (R: right; F: front; L: left). The crab was firmly held in an adjustable clamp, the eyestalks were cemented to the carapace and a small piece of cuticle was removed from the tip of the right eyestalk to access the optic lobe with the microelectrode. (C) Measurement of the escape response. Locomotor activity was studied in a walking simulator device consisting of a water-supported styrofoam ball that could be freely rotated by the animal. Horizontal displacements of the ball were prevented by four set points, provided by the two optical mice used to assess the rotations of the ball and by two flexible sheets located at right angles from each other. The crab was held in position by a weightless rod attached to its carapace that could slide up and down within a guide located above the animal. Both the rod and the guide sleeve had square cross-sections, which prevented the animal from rotating around its yaw axis (further details in Oliva et al., 2007).

where v is the absolute value of the approach speed. By replacing $x(t)$ and using trigonometry, we obtain:

$$\tan(\theta/2) = \frac{l}{L - v \cdot t} = \frac{1}{L/l - v \cdot t/l} = \frac{1}{1/\tan(\theta_0/2) - t/(l/v)}. \quad (3)$$

Eqn 3 indicates that each stimulus is unequivocally characterized by a value of l/v and θ_0.

Because of the limits imposed by the screen's size and distance to the animal's eye, the maximum stimulus expansion was $\theta(t)$=60 deg.

The angular edge velocity of the object, $\psi(t)$, is defined as $\psi(t)=\theta'(t)/2=(1/2)\cdot d\theta/dt$. We used a total of seven looming stimuli (Table 1). For stimuli 1–4, we maintained the approach velocity at v=142.5 cm s^{-1} and varied the size l from 8.5 to 64 cm. The subtended angle of the smallest stimulus at the initial distance was 1.9 deg, which is above the sampling resolution of the crab's eye. In fact, in the lateral part of the eye the resolution reaches values between 0.83 and 1.2 cycles deg^{-1}, corresponding to interommatidial angles between 0.6 and 0.4 deg, respectively (Berón de Astrada et al., 2012). Thus, animals would not have optical limitations to detect differences between the initial sizes of the smaller stimuli used here. For stimuli 5–7, we maintained l=17 cm and varied v from 35.5 to 286 cm s^{-1}. All stimulus speeds used in this study attempted to simulate predators that approach the animal faster than its ability to run away (*Neohelice's* highest escape speed is 35 cm s^{-1}).

Following experiences from our previous studies (e.g. Oliva et al., 2007; Oliva and Tomsic, 2014), we began stimulation after the animal had remained visually undisturbed for 3 min inside the setup. In all trials, the stimulus remained stationary for 30 s at its initial position before starting to increase in size. The inter-trial interval was set to 1 min. The seven stimuli in Table 1 were applied to each animal in a random order.

Electrophysiology

Intracellular recordings from interneurons in the optic lobe were performed in the intact living animal according to methods previously described (Berón de Astrada and Tomsic, 2002). Briefly, the crab was firmly held in an adjustable clamp. The eyestalks were cemented to the carapace at an angle of approximately 70 deg from the horizontal line. A tangential cut performed with a sharp scalpel was made to remove a small piece of thin cuticle (approximately 500 µm in diameter) from the tip of the right eyestalk without causing damage to the ommatidial area.

Table 1. Looming stimulus parameters (see Fig. 1A)

Stimulus	L (cm)	V (cm/s)	l/v (ms)	L (m)	T (s)	θ_0 (deg)
1	8.5	142.5	56	5	3.5	1.9
2	17	142.5	120	5	3.5	3.9
3	32	142.5	225	5	3.5	7.3
4	64	142.5	450	5	3.5	14.5
5	17	35.5	479	5	14	3.9
6	17	71.5	238	5	7	3.9
7	17	286	60	5	1.75	3.9

l is the half-size of the object, v is the approach speed, L is the initial distance, T is the travel time between the initial position to the collision and θ_0 is the initial angular size of the object in degrees. The parameters l/v and θ_0 unequivocally characterize the dynamics of stimulus expansion and are reported for comparisons with the related literature (see Eqn 3).

Journal of Experimental Biology (2016) 219, 3339-3352 doi:10.1242/jeb.136820

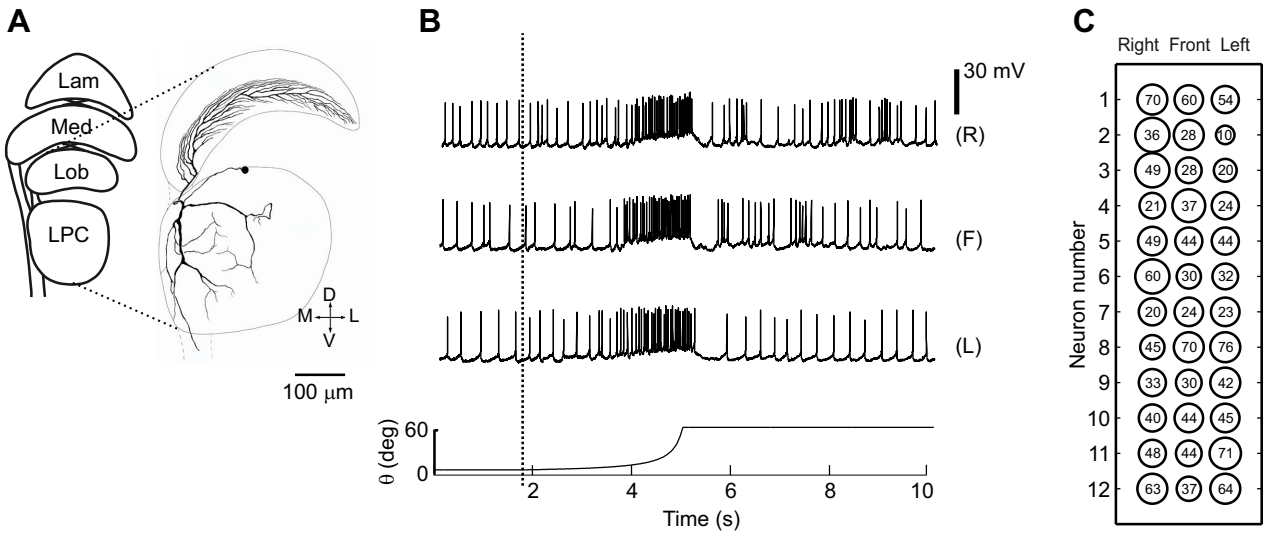

Fig. 2. Receptive field sensitivity of the MLG2 neuron to looming stimuli. (A) Illustration of the location and general morphology of the MLG2 neuron. Lam, lamina; Med, medulla; Lob, lobula; LPC, lateral protocerebrum. (B) Responses of one MLG2 neuron to looming stimulus number 2 (Table 1) presented separately on the monitor to the right (R), front (F) and left (L) of the animal. The vertical dashed line marks the beginning of the stimulus expansion. The lower black curved line represents the time course of the stimulus image expansion. (C) Response magnitude to stimulus number 2 presented on the different monitors for 12 measured neurons. The size of the circles represent the relative intensity of the MLG2 response to each monitor calculated for each neuron as $r(n)=N_{spk}(n)/[N_{spk}(R)+N_{spk}(F)+N_{spk}(L)]$, where N_{spk} is the absolute number of spikes (denoted within the circles) and $n=\{R,F,L\}$ identifies the corresponding monitor. Number of spikes was calculated from the beginning (dashed line) to the end of the stimulus expansion.

The clamp with the crab was held in position within the monitor arrangement (Fig. 1B) using a magnetic holding device. The glass microelectrode was then positioned and advanced through the opening in the cuticle. Microelectrodes (borosilicate glass; 1.2 mm outer diameter, 0.68 mm inner diameter) were pulled on a Brown-Flaming micropipette puller (P-97; Sutter Instrument, Novato, CA, USA) yielding tip resistances of 40–60 MΩ when filled with 3 mol l^{-1} KCl. A bridge balance amplifier was used for intracellular recordings (Axoclamp 2B; Axon Instruments, Union City, CA, USA). The output of the amplifier was monitored on an analogue oscilloscope, digitized at 10 kHz (Digidata 1320; Axon Instruments), and recorded on a computer for subsequent analysis. All intracellular recordings were performed at the membrane resting potential. Without precautions, the monitors located inside a Faraday cage would have generated a significant level of electrical noise in the recordings. We prevented the noise from interfering with the recordings in two ways: (1) by placing a wire mesh immediately in front of each screen and (2) by wrapping the headstage, the electroholder and part of the glass electrode with a dense, properly grounded, metal wire mesh. During the experiment, crabs intermittently moved their legs for a few seconds, which sometimes resulted in losing the impaled cell. These movements, however, did not appear to be associated in time with the presentation of the looming stimulus because they usually occurred within inter-trial periods. Following electrophysiological recordings, crabs remained healthy and no subsequent behavioral differences were observed as compared with un-treated animals.

Classification criteria for MLG2 neurons

Previous physiological characterization followed by intracellular staining and morphological reconstructions allowed us to identify distinguishable features of the MLG2 neuron (Medan et al., 2007). The spontaneous spike activity is approximately 7 Hz. The response to a light pulse generally consists of few spikes to both the onset and the termination of the light, but on–off responses composed of inhibitory postsynaptic potentials were also observed among recordings that appeared to be more dendritic. The response to a moving object can be elicited across an extensive part of the visual field. This response includes a sustained train of action potentials for the duration of the stimulus motion, usually followed, once the motion stops, by a hyperpolarization that suppresses firing for several hundred milliseconds. Likewise, the response to a looming stimulus consists of a progressive increase in firing rate that is usually followed by a period of hyperpolarization and suppression of firing after the cessation of the stimulus. These features allow the MLG2 neuron to be confidently identified. In this study, we recorded and analyzed 12 MLG2 neurons from different animals (no more than two trials per stimulus per neuron).

Behavioral response

The locomotor activity of the crab was investigated in a walking simulator device that has been described in detail elsewhere (Oliva et al., 2007; Oliva and Tomsic, 2012). Briefly, it consisted of a floating styrofoam ball that could be freely rotated by the locomotor activity of an animal, attached in a standing position to a weightless rod through a piece of rubber glued to the animal's dorsal carapace (Fig. 1C). The rod was introduced inside a metal guide, positioned vertically above the ball, where it could slide up and down with little friction. This allowed the animal to feel its own weight and thus adopt its natural posture while performing on the ball. The rod and guide both had square sections, which prevented rotational movements and thus assured that the animal always saw the stimulus with the same side of the eye. Behavior was also monitored by visually observing the animal online through a video camera.

Data analysis

We estimated the instantaneous firing rate by convolving the spike trains with a square window of 50 ms (except in Fig. 4D) and normalizing the resulting waveform such that its integral was equal to the total number of spikes over the entire trial (Gabbiani et al., 1999). To estimate the animal's speed, we convolved the

Journal of Experimental Biology (2016) 219, 3339-3352 doi:10.1242/jeb.136820

instantaneous speed with a 100 ms square window and normalized the resulting waveform (Oliva and Tomsic, 2012). Examples of raw and convolved neuronal and behavioral responses can be seen in Fig. S1. To quantify the intensity of the MLG2 response to each monitor (Fig. 2C), the standardized response r was defined as $r(n)=N_{spk}(n)/[N_{spk}(R)+N_{spk}(F)+N_{spk}(L)]$, where $n=\{R,F,L\}$ identifies the corresponding monitor. The parameters of the different proposed models were estimated by nonlinear least-squares error minimization. Specifically, we used the 'nlinfit' function of MATLAB (The MathWorks, Natick, MA, USA), which minimize the mean square error (between the model's prediction and the experimental data) using the iterative method of Levenberg–Marquardt. Because this optimization method is iterative, we must assign initial values of the parameters to be optimized. We tested normality using the Lilliefors test. The uncertainties of the model parameters were estimated using the bootstrap method (Wasserman, 2004). Data analysis procedures were written in MATLAB.

RESULTS

Responses of the MLG2 neuron to looming stimuli from different directions

Medan et al. (2007) performed the first morphological and physiological characterization of the MLG2 neuron. Fig. 2A illustrates the location and general morphology of this neuron. The dendritic tree consists of several branches that run parallel to each other all along the lateromedial axis of the lobula, thus collecting information from the entire retinotopic mosaic. The physiological receptive field of the MLG2 neuron was previously studied using a black square stimulus with horizontal and vertical translational movements. The neuron responded similarly to the stimulus presented at each one of the screens surrounding the animal, suggesting that its receptive field encompasses the entire visual field of the animal. We further addressed this question by evaluating the looming sensitivity of the MLG2 around different azimuthal positions. Fig. 2B shows the response of one MLG2 neuron to looming stimulus number 2 (see Table 1) presented on the three monitors separately. Responses obtained from 12 neurons (one neuron per animal) were intense and similar for all screens, showing that the looming sensitivity of the MLG2 is quite uniform throughout the azimuthal visual field (Fig. 2C).

Response of MLG2 neurons to different dynamics of approach

Fig. 3 shows the characteristic responses of an MLG2 neuron to different looming stimuli and the average firing rate from 12 neurons. We assessed the response of each neuron to the seven looming stimuli described in Table 1. The response is expressed as firing of action potentials, which frequency gradually augments as the image of the virtual object gets bigger over the animal's retina. In some of the recordings the spikes elicited by visual stimulation appeared on top of a large excitatory postsynaptic potential (EPSP; e.g. see Fig. 2B), whereas in others the component of the EPSP was negligible (Fig. 3). This is due to differences in the site of impalement, which varied from regions close to input sites to regions closer to the spike-initiation zone (Medan et al., 2007).

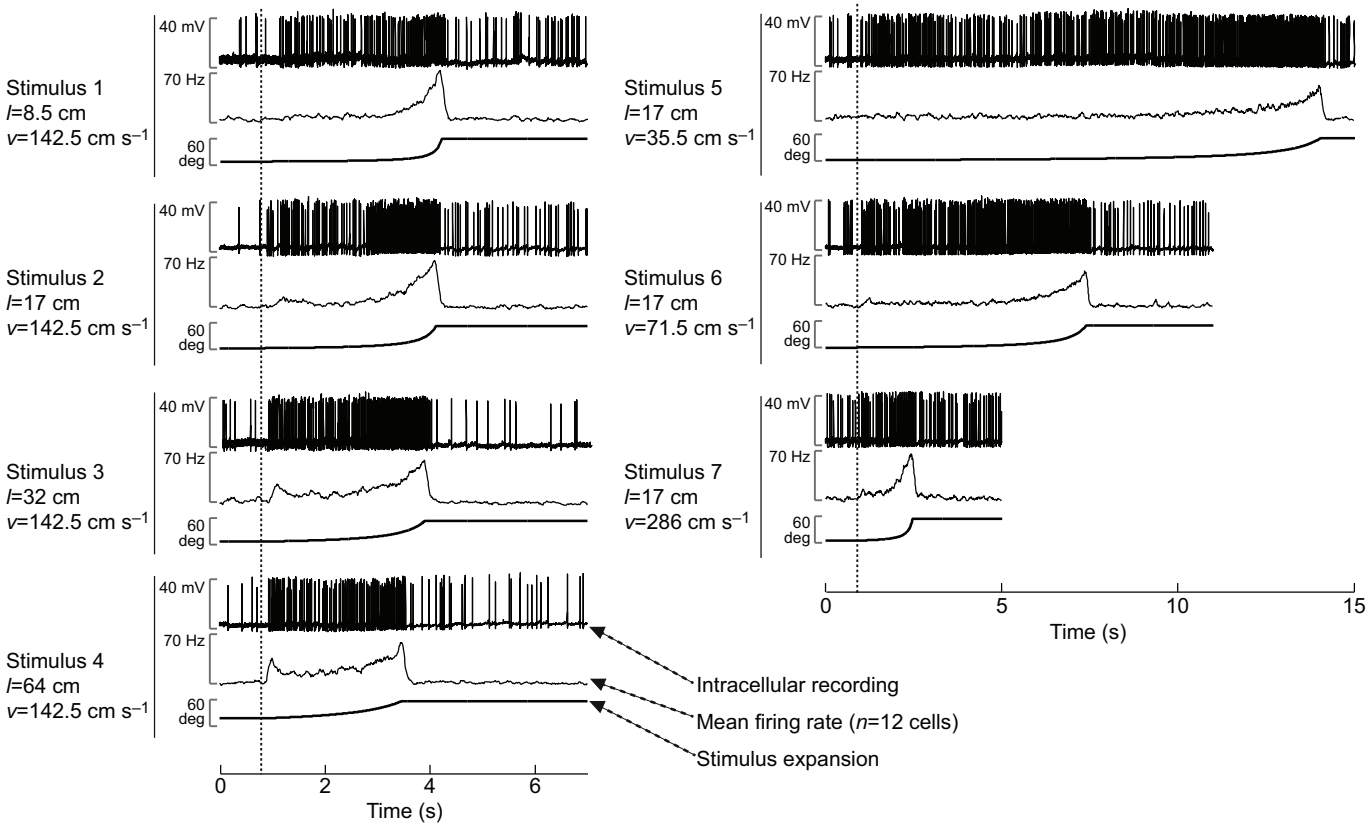

Fig. 3. Response of the MLG2 neuron to different looming stimuli. Left column: responses to stimuli 1–4. Right column: responses to stimuli 5–7 (see Table 1). Upper traces: intracellular recordings from a single MLG2, illustrating the type of responses of this neuron to the seven different stimuli. Middle traces: peristimulus time histograms showing the average spike rate from 12 MLG2 neurons from different animals (no more than two trials per stimulus, per neuron and per animal were included in the analyses). Bottom traces: angular size, $\theta(t)$, of the looming object. Vertical dashed lines signal the beginning of the stimulus expansion. The seven stimuli were applied to each animal from the right monitor, in a random order with an inter-trial interval of 1 min.

Journal of Experimental Biology (2016) 219, 3339-3352 doi:10.1242/jeb.136820

Another diagnostic mark observed in different recordings of MLG2 to looming stimuli was the presence of a transient constituent of the response at the beginning of the expansion. This effect can be observed in Fig. 3, mostly with stimuli 3 and 4 (θ_0=7.3 and 14.5 deg, respectively).

Physiological mechanisms regulating the response of the MLG2 to looming stimuli

In this section we study some physiological phenomena previously observed in the locust's LGMD neuron (Jones and Gabbiani, 2010, 2012) and in MLG1 neurons of the crab (Oliva and Tomsic, 2014), which proved to be relevant to the codification of looming stimuli.

Dependence of the excitation latency on the stimulus angular velocity

Recent studies have investigated the action of the excitatory presynaptic circuit on the LGMD by recording from the photoreceptors and the lamina monopolar cells (Jones and Gabbiani, 2010, 2012). The visual stimulus used in these investigations was a border moving at different uniform velocities θ' through the neuronal receptive field. The latency of the peak response in lamina monopolar cells was found to diminish as the border velocity increased. On this basis, a change in the excitation latency δ_e between the initiation of the looming stimulus and the beginning of the MLG2 response is anticipated for stimuli with different dynamics. For each trial, δ_e is identified as the interval between the initiation of the stimulus expansion and the beginning of the neuronal response. The response onset was chosen as the time at which the firing frequency doubled the highest frequency attained in the 2 s prior to stimulation. The analysis was performed for stimuli 3, 4 and 7, because these were the stimuli for which we undoubtedly identified the beginning of the neural response in most of the individual recordings (Fig. 3). As shown in Fig. 4A, we obtained a relationship between the latency in the MLG2 response and the looming stimulus angular velocity θ' corresponding to the first 10 ms of the expansion:

$$\delta_e = 0.5\,\text{deg}/(\theta' + 0.01\,\text{deg}\,\text{s}^{-1}) + 0.04\text{s}. \quad (4)$$

This effect was taken into account in our proposed model for MLG2 synaptic excitation (more details in the Appendix).

Synaptic inhibition

As previously observed in MLG1 neurons (Oliva and Tomsic, 2014), two pieces of evidence support the existence of synaptic inhibition acting on MLG2 neurons. First, Fig. 4B shows the average off-response to a flashlight. With this stimulus, an excitatory response (with or without spikes) followed by an inhibitory response was regularly detected (dotted ellipse). Second, at the end of looming stimuli, the MLG2 shows an inhibitory response (Fig. 2B, 4C; see also fig. 6I in Medan et al., 2007).

Relationship between membrane potential and firing frequency in the MLG2 neuron

The model proposed by Jones and Gabbiani (2012) for the biophysical implementation of the computation performed by the locust's LGMD neuron in response to looming stimuli includes two aspects: (1) the effect of synaptic excitation and inhibition at the level of the LGMD's membrane potential (see below) and (2) the transformation of the membrane potential into the LGMD's firing rate by a nonlinear input–output relationship. To evaluate the relationship between the MLG2 membrane potential and its firing rate we employed a median filter to cut off the action potentials

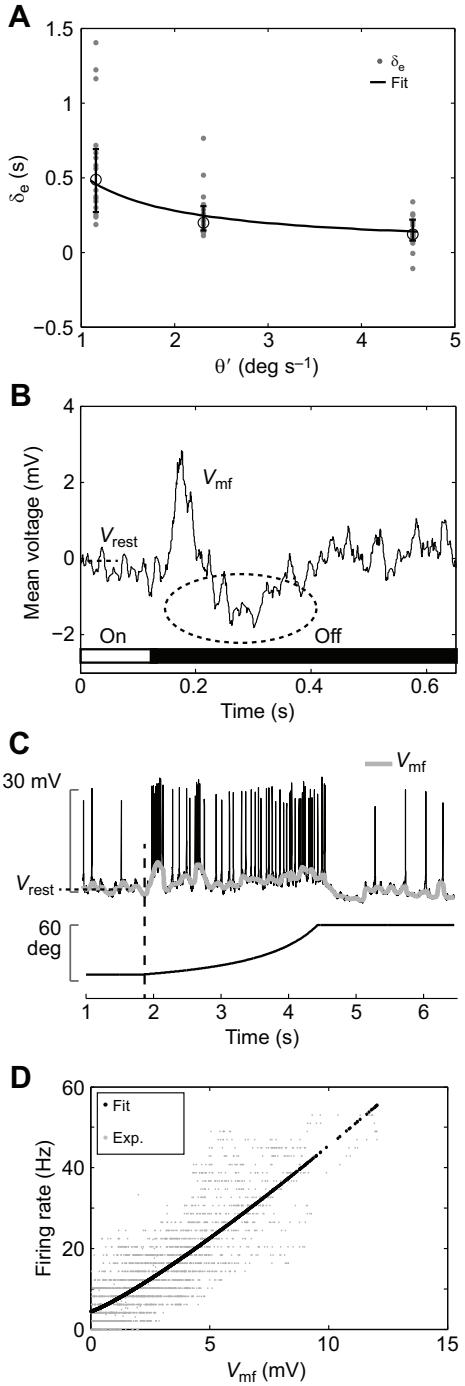

Fig. 4. Physiological mechanisms regulating the response of the MLG2 neuron to looming stimuli. (A) Excitation delay δ_e as a function of the stimulus' angular velocity (10 neurons from 10 different animals; filled circles represent single trials, no more than two trials per cell). The delay decreased with increasing stimulus angular velocity θ'. Empty circles represent medians and whiskers indicate the interquartile range. The black trace shows the fit according to Eqn 4 (r^2= 0.7). (B) Mean filtered membrane potential (V_{mf}) in response to an off stimulus (10 neurons, from different animals, one trial per cell). An inhibition (dashed ellipse) following the brief excitation can be observed. The resting potential V_{rest} is indicated by a horizontal dashed line. (C) V_{mf} (light gray) was estimated by applying a median filter (width 250 ms, sliding step 50 ms) to remove the action potentials. Firing frequency was estimated by convolving the spike trains with a square window (width 500 ms, sliding step 50 ms). (D) Covariation of the firing rate and V_{mf} for one neuron. The black circles show the fit according to Eqn 5 (r^2= 0.7). The obtained least-squared parameters for this neuron were: k_r=2.8 Hz, a_r=1.17 and R_0=4.4 Hz.

Journal of Experimental Biology (2016) 219, 3339-3352 doi:10.1242/jeb.136820

(Fig. 4C). Then, we represented the firing frequency as a function of the membrane potential. A cursory inspection of Fig. 4D indicates a covariation between the value of the membrane potential and the firing frequency. A clear mapping (denoted as f_R) between the two variables could be fitted with a power law input–output function (Gabbiani et al., 2002):

$$R_{MLG2} = f_R(V_{mf}) = k_r \cdot (V_{mf})^{a_r} + R_0, \quad (5)$$

where R_{MLG2} is the firing rate, V_{mf} is the filtered membrane potential (relative to the resting potential V_{rest}), and k_r, a_r and R_0 are constants. Observe that the exact fit function (specially the exponent) is expected to depend on how close the recording is taken from the spike initiation zone of the neuron. We fitted the model of Eqn 5 for different neurons (n=3; r^2=0.65±0.15) to obtain: k_r=7.7±3.5 Hz, a_r=1±0.2 and R_0=5.8±3.2 Hz (mean±s.d.). This information was incorporated into our proposed model for the synaptic excitation of the MLG2 neuron (more details in the Appendix).

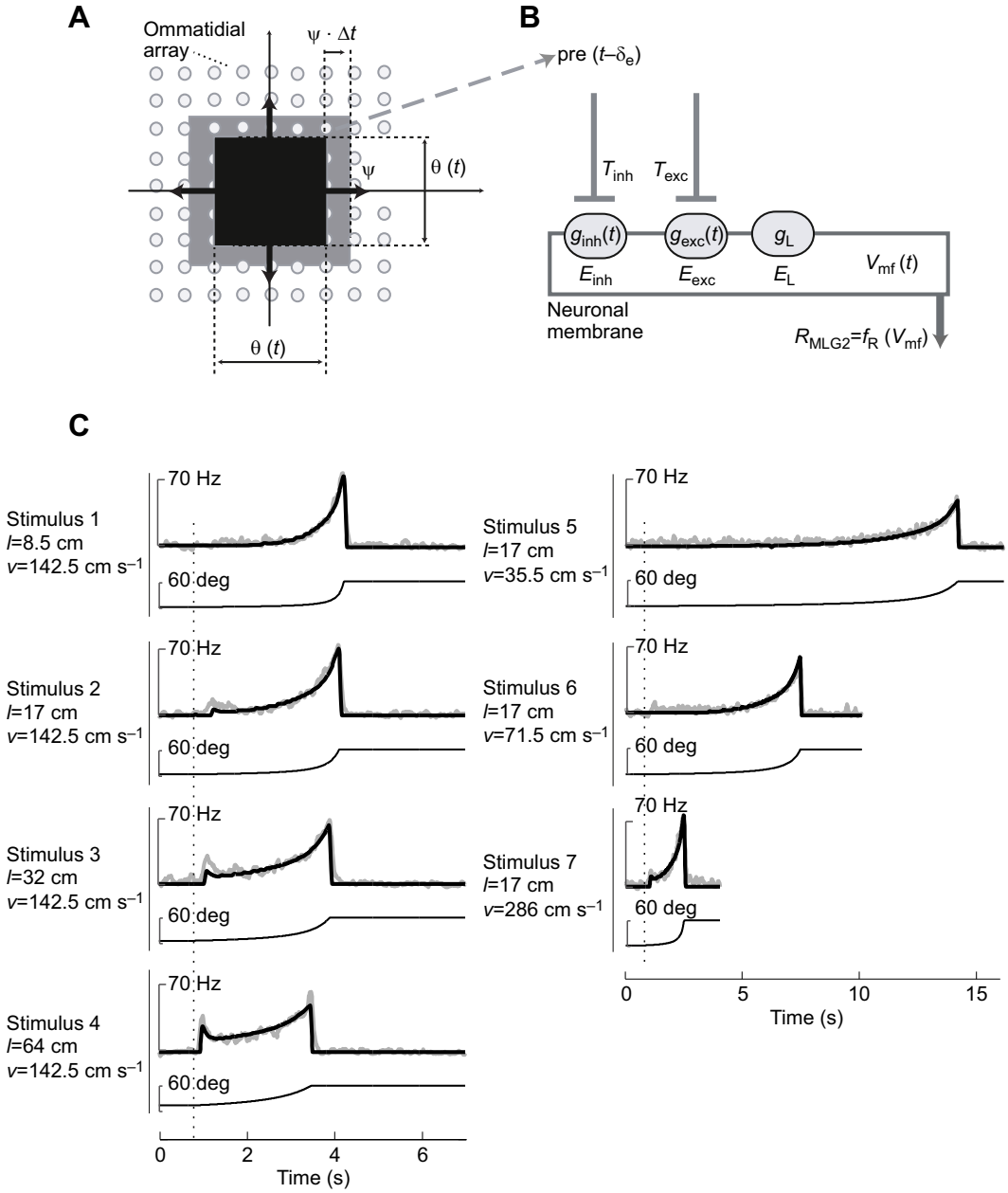

Fig. 5. Plausible biophysical model of looming detection in the MLG2 neuron. (A) Expanding black edges move with an angular velocity ψ through the ommatidial array (small light gray circles). In every monitor's new frame, the square increases its angular size, θ(t) (gray square). Every new frame, the angular size is increased by 2ψ·Δt, changing the upper, lower, left and right edges' positions symmetrically. (B) The proposed model assumes that when the object is expanding; the signal of presynaptic columnar channels, *pre*(t–δe), activates excitatory and inhibitory synapses with conductance (g_{exc}, g_{inh}) acting on the dendrites of the MLG2 (more details in the Appendix). The dynamic balance between these conductances determines the filtered membrane voltage, V_{mf}, according to Eqn A4. Finally, the firing rate R is calculated using Eqn 5. (C) Average data and model predictions of the firing rate of the MLG2 neuron. Left column: responses to stimuli 1–4. Right column: responses to stimuli 5–7. Peristimulus time histograms (gray traces) show the mean spike rate from 12 MLG2 neurons. Spikes were convolved with a 50 ms square kernel. Black traces superimposed on the measurements represent the firing rate predicted by the model. The angular size, θ(t), of the looming object is represented by the black curved line at the bottom of each panel. Dotted vertical lines signal the beginning of the stimulus expansion.

Journal of Experimental Biology (2016) 219, 3339-3352 doi:10.1242/jeb.136820

Biophysical model of MLG2 for looming detection

Our model for looming detection in the MLG2 neuron has been inspired by computational models for the locust's LGMD neuron (Rind and Bramwell, 1996; Peron and Gabbiani, 2009; Jones and Gabbiani, 2012). Similar to our model for MLG1 neurons (Oliva and Tomsic, 2014), the model for the MLG2 assumes that each columnar pathway supplies information on variations in luminosity for each ommatidium (Fig. 5A). The signal of presynaptic columnar pathways, $pre(t–\delta_e)$ (see Eqn A1 in the Appendix), is divided into excitatory and inhibitory synapses with different temporal dynamics. This produces a dendritic sublinear transformation of the presynaptic signal (see Eqns A2, A3 in the Appendix). The effects of both synaptic conductances (g_{exc}, g_{inh}) are added at the neuron, which is modeled as a unique compartment (Fig. 5B). According to our model, the filtered membrane potential V_{mf} is a function of the dynamic balance of the synaptic conductances and becomes transformed by the firing rate mechanism (Eqn 5) (further model details in the Appendix).

Parameters that could not be disclosed using intracellular recording information were approximated by nonlinear square error minimization between the mean firing frequency and model predictions. Fig. 5C shows that our simplified biophysical model confidently predicted the neuronal firing rate during the whole expansion for all the stimuli tested. The model predicts that the initial phasic responses are due to a dynamic balance in favor of fast synaptic excitation. Subsequently, the slow synaptic inhibition acts on the neuron reducing their activity. These initial phases became more apparent with large stimuli (see stimuli 3 and 4). Then, when the expansion reaches fast angular velocities, the effect of excitation again surpasses inhibition, producing a sustained firing rate increase associated with the looming response. Finally, upon completion of the expansion, a fall owing to the action of inhibition occurs (see fig. 8C in Oliva and Tomsic, 2014).

Phenomenological model of the MLG2 response to looming stimuli

Responses to looming stimuli of LSNs from different animals have been described in terms of phenomenological models. These models imply input–output relationships of the type $R(t)=F[z(t–\delta_n)]$, where z is an input optical variable, $R(t)$ is the neuronal firing rate and δ_n is a constant neuronal delay. The optical variables most commonly used are angular size $\theta(t)$, angular velocity $\theta'(t)$ and angular acceleration $\theta''(t)$ (Oliva, 2015). Therefore, we thought to identify a simple optical variable and a mathematical function that predicts the firing frequency of the neural response to looming stimuli. This demanded the evaluation of responses to stimuli with different sizes and speeds of approach, hence showing distinctive expansion dynamics. For this analysis we used the firing rate measurements following $\Delta\theta>7$ deg, which, according to the behavioral analyses, corresponds to the threshold value of angular increment associated with the start of the escape run (Oliva and Tomsic, 2012). Fig. 6 shows the average firing rate as a function of the angular size $\theta(t–\delta_n)$, angular velocity $\theta'(t–\delta_n)$ and angular acceleration $\theta''(t–\delta_n)$, assuming a neural response delay of δ_n=35 ms at 22–24°C according to Medan et al. (2007) (same temperature as in the present study) and to our delay measurements for angular velocities greater than 5 deg s^{-1} (Fig. 4A). The data show that the firing rate is not a function of the angular size, as for any particular value of θ (Fig. 6A) the firing rates elicited by the different stimulus dynamics are dissimilar. However, when angular velocity (Fig. 6B) or angular acceleration (Fig. 6C) are considered, the firing rate appears to be independent of the stimulus dynamic. To distinguish which of these variables best describes the neural response of the MLG2, we fitted the following phenomenological model:

$$R_{MLG2}(t) = F_{MLG2}[z(t-\delta_n)] = \frac{R_{max}\cdot z(t-\delta_n)}{z_{50\%}+z(t-\delta_n)} + R_0. \quad (6)$$

To quantify the goodness of the fits, we calculated the fitting error using nonlinear least square optimization (see Materials and methods). The absolute errors (E; Hz) for the variables θ, θ′ and θ″ were, respectively: E_θ=8.9±0.2, $E_{\theta'}$=2.1±0.1 and $E_{\theta''}$=3.4±0.1. Therefore, the model of Eqn 6 that produced the best fit of the firing rate corresponded to z=θ′, a result similar to that found in the crayfish's jittery movement fibers (Glantz, 1974) and the ρ neurons in pigeon (Sun and Frost, 1998). The optimal parameter values

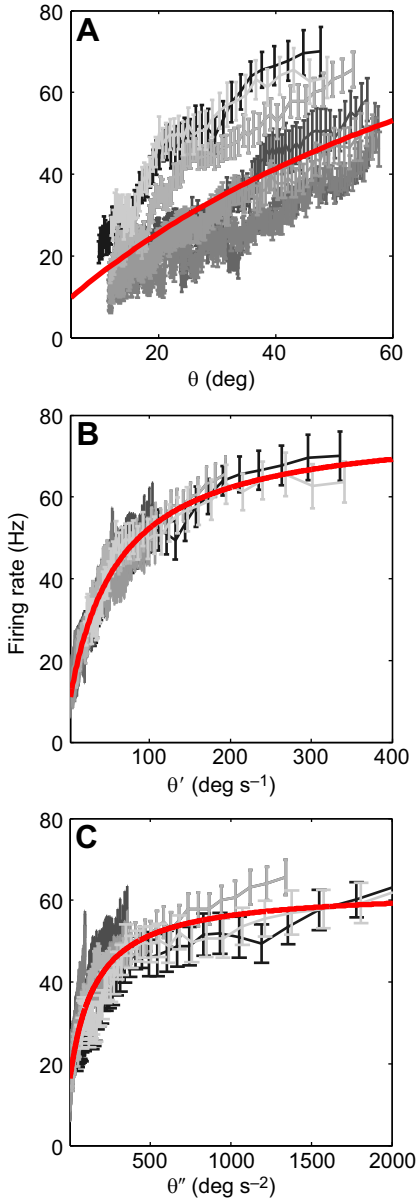

Fig. 6. Average firing rate and optimal fits for MLG2 phenomenological models. Data obtained for the seven stimuli of Table 1 plotted as a function of three different optical variables: (A) angular size θ, (B) angular velocity θ' and (C) angular acceleration θ''. Red lines correspond to the fits using Eqn 6.

Journal of Experimental Biology

Journal of Experimental Biology (2016) 219, 3339-3352 doi:10.1242/jeb.136820

obtained for this model were: R_{max}=70±2 Hz, $z_{50\%}$=60±5 deg s^{-1} and R_0=8±1 Hz.

Relationship between MLG2 activity and the speed of escape running

After having examined the response of the MLG2 neuron to looming stimuli, we analyzed its relationship with the animals' speed of escape to the same stimuli. Fig. 7 shows the mean firing rate of MLG2 and the mean running speed (light and dark gray traces, respectively) for each of the stimuli tested. A cursory inspection of these data focused on the time between the escape initiation and the highest speed of run (red box) suggests a close correspondence of the temporal courses between the dynamic of stimulus expansion, the neuronal firing rate and the behavioral performance. Compare, for example, the responses to stimuli representing a slow and a fast object approach (stimuli 5 and 7, respectively). The faster stimulus induced an earlier and faster increase in the neural firing rate, as well as an earlier and faster increment in the speed of run than the slower stimulus. Likewise, the dynamics generated by a small or a large object approaching at the same velocity (stimuli 1 and 4, respectively) are reflected by the time and intensity course of both the neuronal and the behavioral response. The matching between the dynamic of stimulus expansion, the neuronal activity and the speed of escape suggests that relevant information on the actual stimulus situation could be encoded and conveyed downstream by the firing rate of the MLG2 to regulate the speed of escape. To further analyse this possibility, we attempted to predict the running speed in response to looming stimuli using the firing rate of the MLG2.

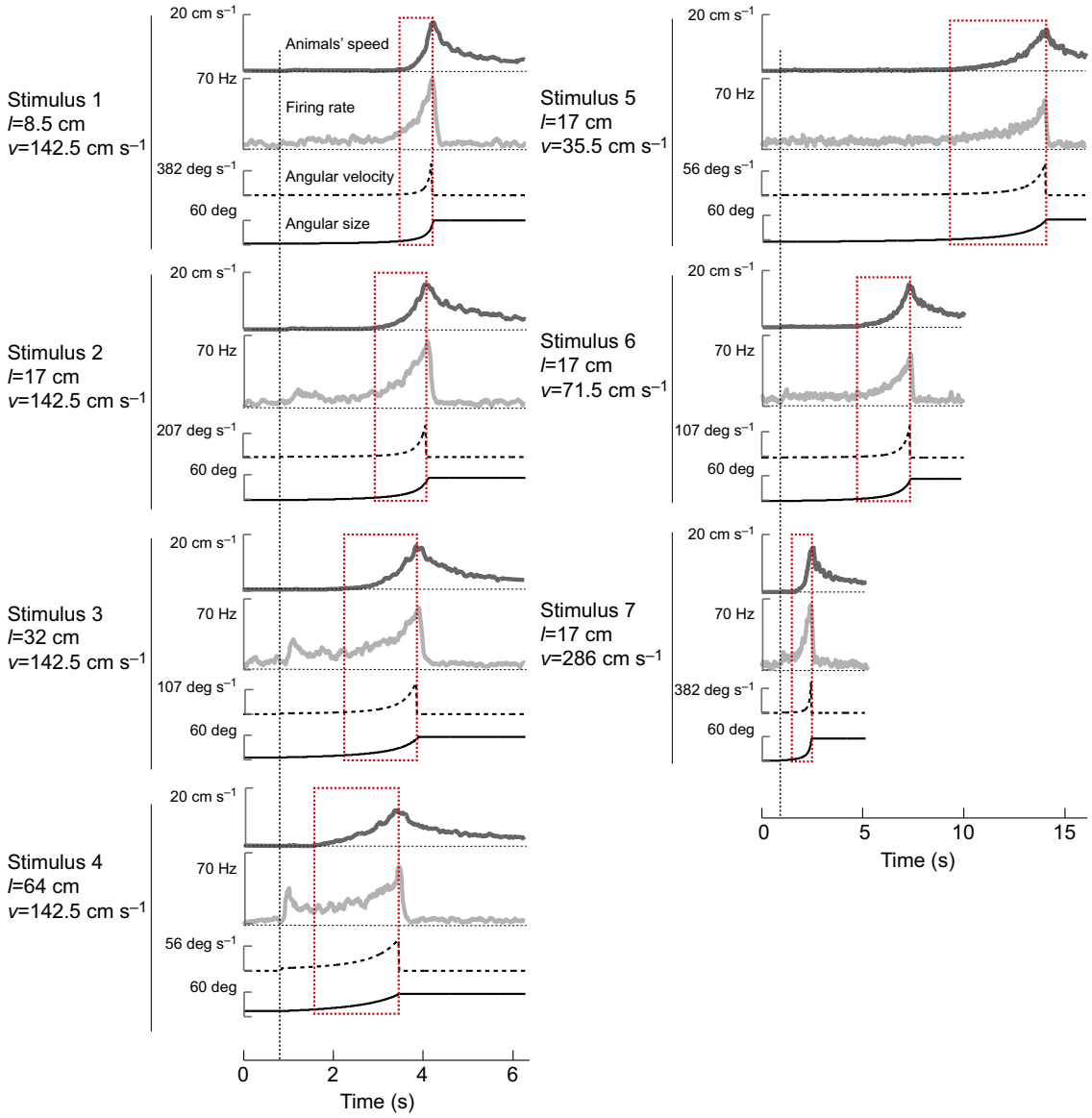

Fig. 7. Firing rate of MLG2 neurons and animals' speed. Left column: responses to stimuli 1–4. Right column: responses to stimuli 5–7. Peristimulus time histograms at the center of each panel (light gray traces) show the mean spike rate from 12 MLG2 neurons (not more than two trials per stimulus, per neuron, per animal). Spikes were convolved with a 50 ms square kernel. The mean animals' speed, $v_c(t)$, is represented at the top of each panel (dark gray traces). Angular velocity $\theta'(t)$ and angular size $\theta(t)$ of the looming stimulus are, respectively, represented by the dashed and continuous black curved lines at the bottom of each panel. Note the differences in angular velocity scale for the different stimuli. Dotted vertical lines signal the beginning of the stimulus expansion. The red boxes highlight the temporal courses of correspondence between the dynamic of stimulus expansion, the neuronal firing and the behavioral performance.

Journal of Experimental Biology (2016) 219, 3339-3352 doi:10.1242/jeb.136820

In Oliva and Tomsic (2012) we have shown that the escape response to looming stimuli of the crab consists of a threshold-type decision for initiating the run, followed by adjustments of the running speed concurrently with the dynamic of the stimulus expansions. The escape decision and the regulated speed mechanism were described by a phenomenological input–output function f_{IO} that predicted the crab speed, $v_c(t)$, as a function of an optical variable, $u(t–\delta)$, evaluated δ milliseconds earlier (Oliva and Tomsic, 2012). The optical variable $u(t)$ was the product of the angular increment since the onset of expansion, $\Delta\theta(t)=\theta(t)–\theta_0$, and the stimulus angular velocity, $\theta'(t)$:

$$u(t) = [\Delta\theta(t) - \Delta\theta_{esc}] \cdot \theta'(t)$$
$$v_c(t) = f_{IO}[u(t-\delta)] = v_{max} \cdot \frac{u(t-\delta)}{u_{50\%} + u(t-\delta)} \quad (7)$$
$$\text{if} \quad u(t-\delta) \geq 0$$
$$v_c(t) = 0 \quad \text{if} \quad u(t-\delta) < 0.$$

The parameter $\Delta\theta_{esc}$=7 deg was a threshold independent of looming stimulus dynamics and $u_{50\%}$ was the value of the variable u when the animal reaches 50% of v_{max} (the maximum velocity of escape). Given this previous result and the relationship between the firing rate of the MLG2 and the stimulus angular velocity described in Eqn 6 and Fig. 6, we replaced the time-dependent angular velocity $\theta'(t)$ by the experimental firing rate of MLG2. Because the response of the MLG2 entails a nonlinear transformation of θ' (Eqn 6), we adjusted the model parameters of Eqn 7 to obtain v_{max}=24±1 cm s^{-1}, $u_{50\%}$=1615±130 deg s^{-1}. Fig. 8 shows the behavioral measurements and the predictions of the model for the situation tested. The correlation between the actual behavioral records and the values of running speed predicted by the model using the MLG2 firing rate is high (ρ=0.98).

DISCUSSION

VGCABs have been investigated in different animal species. In most studies, the avoidance response has been associated with the moment in which an optical parameter of the looming stimulus reaches a threshold value. Some responses can develop in stages, with a threshold value associated with each stage. The optical parameters that have been most commonly associated with the response time are: (1) angular size, e.g. in locusts (Fotowat and Gabbiani, 2007), flies (Card and Dickinson, 2008) or fish (Dunn et al., 2016); (2) angular increment, e.g. in crayfish (Glantz, 1974); and (3) a combination of angular size and velocity, which allows an estimation of the time to collision, e.g. in flies (Wagner, 1982). Whereas some VGCABs can rely on threshold values to be triggered and properly executed, others operate under continuous visual control. In the latter case, the change of an optical parameter (or a combination of parameters) is constantly assessed and used by the animal to regulate the corresponding visuomotor transformation

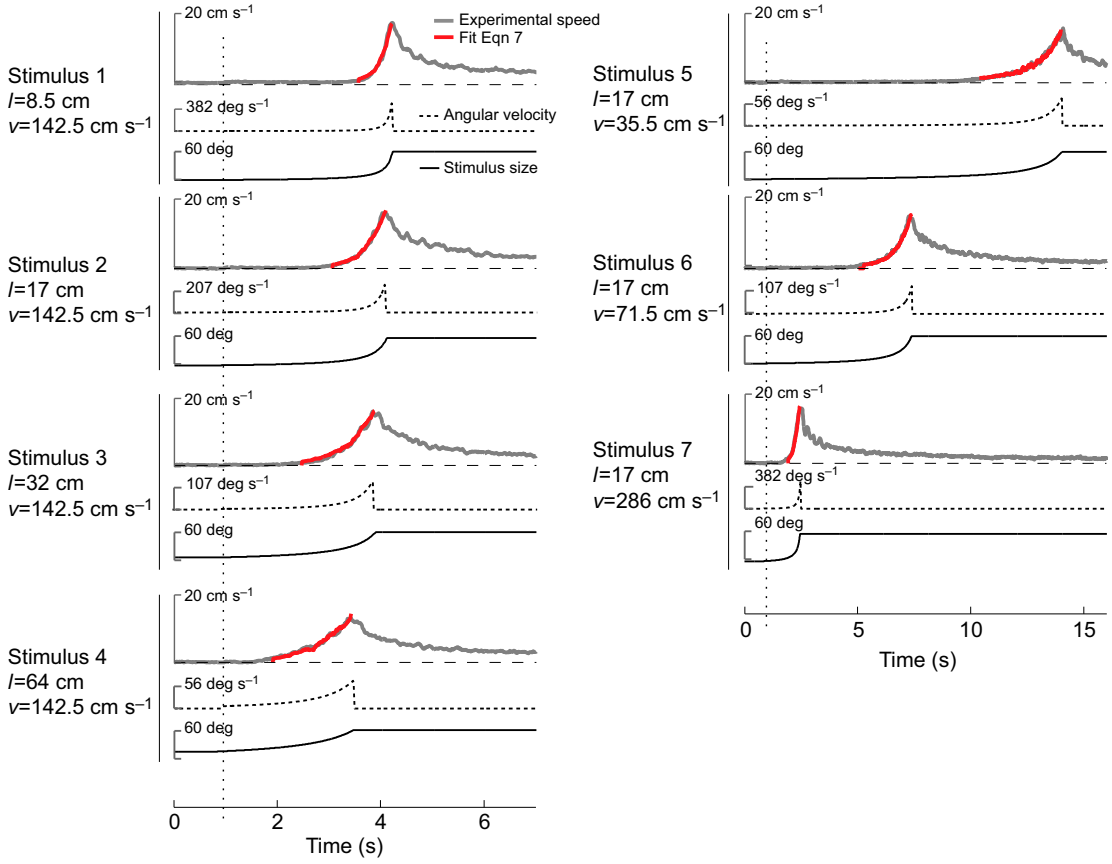

Fig. 8. Fits of the animals' speed using the phenomenological model of Eqn 7. Left column: responses to stimuli 1–4. Right column: responses to stimuli 5–7. The average animals' speed, $v_c(t)$ elicited by each looming stimulus is represented by the dark gray trace. Red lines correspond to the fits using Eqn 7, but replacing the time-dependent angular velocity $\theta'(t)$ by the experimental firing rate of MLG2. The angular velocity $\theta'(t)$ and the angular size $\theta(t)$ of the looming stimulus are represented by the dashed and continuous black curved lines at the bottom of each panel, respectively. Dotted vertical lines signal the beginning of the stimulus expansion.

Journal of Experimental Biology

Journal of Experimental Biology (2016) 219, 3339-3352 doi:10.1242/jeb.136820

(Srinivasan and Zhang, 2004). LSNs have been studied in connection with VGCABs based on threshold detections, but to the best of our knowledge there are no studies of LSNs in connection to VGCABs operating under continuous regulation. Because we have previously found that when escaping from looming stimuli, crabs regulate their running speed according to the dynamic of stimulus expansion (Oliva and Tomsic, 2012), we investigated and here showed results of an LSN, the MLG2 neuron, that can participate in such a regulated visuomotor transformation.

Phenomenological account of the MLG2 response to looming stimuli

Descriptions of LSNs usually began with a phenomenological account of the neuronal response as a function of a single optical variable (or a combinations of variables) of the looming stimulus. Studies focused on the response of a single morphologically well-identified type of neuron, such as the LGMD of the locust (e.g. Fotowat and Gabbiani, 2011), or on population responses of neurons, such as those recently described in the optic tectum of the zebrafish (Dunn et al., 2016). In both examples, the neural response encodes the dynamic of the stimulus expansion, and the activity reached at a fixed angular size was associated with the stimulus threshold of the corresponding avoidance behavior. Thus, although these neurons may encode the stimulus expansion in a continuous fashion, the associated behaviors use threshold information.

Just as previously done for LSNs from the crayfish (Glantz, 1974) and pigeons (Sun and Frost, 1998), the firing rate of the crab's MLG2 can be described as a function of the angular velocity θ' of the stimulus expansion (Fig. 6, Eqn 6). Because stimulus angular velocity is one of the optical parameters used by the crab to regulate its running speed in response to looming stimuli (Oliva and Tomsic, 2012), the MLG2 is a good candidate to be involved in speed regulation.

Physiological model of the MLG2 response to looming stimuli

Following the phenomenological analyses of the MLG2 computation, we investigated the physiological processes that support this computation. The most compelling studies on this subject have been carried out in the LGMD neuron of the locust, using biophysical computational models (Rind and Bramwell, 1996; Peron and Gabbiani, 2009; Jones and Gabbiani, 2012). In the present study, we showed that MLG2 shares several physiological features with the locust's LGMD and with the crab's MLG1. Based on our experimental results, we modified a biophysical model (Oliva and Tomsic, 2014) and extended it to describe the coding of looming stimuli in the MLG2. Our simplified description of the physiological mechanisms involved in coding looming stimuli confidently predicted the neuronal firing rate during the whole expansion for all the stimuli tested (Fig. 5). It also describes the transient initial response component observed with larger stimuli. Therefore, the model heuristic value contributes to the understanding of the biophysical processes underlying looming responses of the MLG2 neuron.

Relationship between MLG2 firing activity and speed of escape to looming stimuli

Contrasting with the progress made in understanding the multistage avoidance response to looming stimuli in the locust, where distinct features of the increasing firing activity of the LGMD neuron could be related to different stages of the behavioral response (Santer et al., 2008; Fotowat and Gabbiani, 2007; Fotowat et al., 2011; Silva et al., 2015), almost no advances have been made in relation to a continuously regulated response to looming stimuli in any animal.

The crab's avoidance behavior to looming stimuli is composed of a threshold-type decision for launching the escape run, followed by a visually regulated mechanism for the running speed (Oliva and Tomsic, 2012). The escape decision and regulated speed mechanism can be explained by a phenomenological input–output relationship, where the crab's speed, $v_c(t)$, is associated with an optical variable resultant from the multiplication of the angular increment since the beginning of expansion, $\Delta\theta(t)=\theta(t)-\theta_0$, and the stimulus angular velocity, $\theta'(t)$. Fig. 6 shows that MLG2 neurons consistently encode the stimulus angular velocity during the running phase of the escape response. Therefore, in our input–output function of the crab's speed, we replaced the values of the stimulus optical variable $\theta'(t)$ by the firing rate values of the MLG2, and obtained remarkably good predictions of running speeds for all the stimulus dynamics (Fig. 8). These results support the notion that the looming information encoded in the activity of the MLG2 serves to regulate the speed of escape run. However, it must be noted that according to our phenomenological input–output model, angular velocity is not the only parameter used by the crab to regulate its speed of escape. The crab also uses the angular increment. We still do not know which neurons compute this parameter, neither do we know the way in which they could do this.

Uncoupling between MLG2 firing rate and escape performance

During looming stimulation, MLG2 activity matches the crab's speed of run from the time of escape initiation to the maximum speed of escape. However, the neuronal and behavioral activity are clearly uncoupled before and after that window. When confronted with large stimuli (e.g. our stimuli 3 and 4), MLG2 responds with a transient but noticeable increase of the firing rate. This transient response component to large looming stimuli also happens in the LGMD of the locust, where it has been interpreted to be caused by the sudden acceleration in the edges of the stimulus that occurs at the very beginning of the stimulus motion (Rind and Simmons, 1992). The transient increase of firing rate does not appear to be associated with any particular behavioral component. In the crab, it occurs much earlier than the escape initiation (see Fig. 7). This disengagement is not surprising, because escape initiation only occurs after the stimulus reaches an angular increment threshold of 7 deg (Oliva and Tomsic, 2012), which in our stimuli happens by the time the high firing rate of the initial transient component has already declined. In other words, the MLG2 firing activity may be necessary but not sufficient to command the behavior.

The MLG2 and the behavioral performance were also shown to be disengaged following the end of stimulus expansion, when the firing rate of the neuron immediately dropped to baseline whereas the crab slowly decelerated (see Fig. 7). A plausible interpretation would be that the stimulus information conveyed by the MLG2 (and likely by other neurons too; see below) serves to boost up a central pattern generator that, after the end of the stimulus expansion and the corresponding cessation of neuronal firing, continues being active for a while.

Different LSNs working together

Investigations in the locust highlighted the role of the LGMD in the avoidance responses to looming stimuli, but also showed that other LSNs, such as the LGMD2 (Rind, 1996), are likely involved with the execution of those responses (see also Gray et al., 2010; Fotowat

et al., 2011; Sztarker and Rind, 2014). While escaping from an approaching object, crabs continuously regulate their speed (Oliva and Tomsic, 2012) and direction of run (Medan et al., 2015). These complex visuomotor transformations can hardly be under the control of a single class of LSN. We have previously shown that the response of MLG1 neurons follows the looming stimulus dynamics, and that their firing rate can be simply described as a function of the stimulus angular velocity. However, this capacity of MLG1s to encode angular velocity works well only until the stimulus reaches a size of 35 deg, i.e. during the early stage of escape (Oliva and Tomsic, 2014). MLG1 neurons form a system of 16 retinotopically organized units that map the 360 deg of azimuthal space (Medan et al., 2015). Of note, crabs can steer the course of escape straight away from a visual danger wherever the stimulus is situated in the 360 deg field of view. They adjust the escape course with a precision of less than 1 deg (Medan et al., 2015). Thus, an activity code (reflecting stimulus dynamics under 35 deg) and a place code (reflecting stimulus location anywhere around the animal) were proposed to be embedded in the MLG1 system (Medan et al., 2015). These two codes would cooperate to perform the visuomotor transformations involved in controlling the crab's initial speed and the course adjustment when escaping from a visual danger. Our current results on the MLG2 show that the response profile of this neuron (i.e. the temporal course of its spiking activity) reflects the exact dynamic of looming stimuli and, even more important, its incorporation into a phenomenological input–output model allows us to faithfully predict the running speed of the escape response until the end of expansion (Fig. 8).

We know that the axon of MLG2 exits the optic lobe towards the supraesophageal ganglion, where it presumably contacts premotor nuclei, but we still do not know its actual postsynaptic target. This might cast some doubts on the involvement of this neuron in the visually elicited running response. However, given the strong relationship revealed between the firing activity of the neuron with the visual input (stimulus angular velocity) as well as with the motor output (animal running speed) for a wide range of looming dynamics, we find it untenable that this neuron would not play a central role in the visually guided escape of the animal.

The precise role played by MLG1 and MLG2 elements and the way they may interact together to convey downstream information regarding the position and dynamic of approaching stimuli is still to be determined. Our simplified working hypothesis is that the 16 MLG1 neurons, with their limited receptive fields that in combination cover the 360 deg azimuthal positions (Medan et al., 2015), are involved with the fine directional tuning of the escape run; whereas the MLG2 neuron, with its very extensive receptive field and its firing activity matching the speed of the run until the end of the stimulus expansion, is involved with the regulation of the running speed.

Appendix

Simplified biophysical model of the MLG2 response to looming stimuli

Based on the data described above, our previous results with the MLG1 (Oliva and Tomsic, 2014) and results from other authors with the LGMD neuron of the locust, we propose a biologically plausible model of computation performed by the MLG2 neuron of the crab (Fig. 5). We assumed that the most relevant physiological mechanisms shaping the response of the MLG2 are: (1) a dynamic balance between synaptic excitation and inhibition, (2) a varying presynaptic delay dependent on angular velocity and (3) a mapping between filtered membrane voltage and firing rate (Fig. 5). As the expanding black edges move through the ommatidial array with angular velocity ψ (Fig. 5A), the columnar channels impinging on the MLG2 have a response proportional to ψ, approximated by $f_{LMC}=(\psi/\psi_{max})^{a_{LMC}}$, where ψ_{max} is a constant selected to obtain an adimensional and normalized function f_{LMC}, and a_{LMC} is an exponent associated with a nonlinear response. Additionally, we assumed that these columnar channels are activated if the edge's angular velocity ψ surpasses a value of ψ_{min}.

As shown in Fig. 2, MLG2 looming sensitivity is rather uniform throughout its large receptive field. Consequently, unlike in our previous model for the MLG1 neuron, the MLG2 model does not require the introduction of a receptive field sensitivity function. Therefore, we propose that the total presynaptic signal acting on the MLG2 dendrites during the image frame (t, $t+\Delta t$) is proportional only to: (1) the number of ommatidia with an on–off transition along the expanding border (gray border in Fig. 5A) and (2) the intensity of the columnar channel responses previously described by $f_{LMC}(\psi)$. If we use the planar approximation to the eye surface, we can write for the total presynaptic signal:

$$pre(t) = k_{pre} \cdot 4\theta(t) \cdot \psi(t) \cdot \Delta t \cdot f_{LMC}[\psi(t)], \quad \text{(A1)}$$

where k_{pre} is a constant selected such that the $pre(t)$ signal was normalized to the maximum value reached with stimulus 1 (which is the maximum value obtained for all stimuli). The presynaptic signal $pre(t)$ is divided in two pathways (excitatory and inhibitory) acting on the MLG2 neuron (Fig. 5B). The variables T_{exc} and T_{inh} are proportional to the amount of the neurotransmitter released at the presynaptic space. Their time evolution is modeled as first-order dynamics:

$$\tau_n \cdot \frac{dT_n}{dt} + T_n = pre(t - \delta_e), \quad \text{(A2)}$$

where n={exc, inh} corresponds to excitatory and inhibitory pathways, δ_e is the excitation latency (see Eqn 4) and τ_n corresponds to the excitatory and inhibitory time constants. We further assumed that the reaction between neurotransmitter and postsynaptic receptors instantly reaches steady state (Destexhe et al., 1994). Therefore, the postsynaptic conductances are proportional to the amount of neurotransmitter (T_n) released as follows:

$$g_n(t) = g_{n,max} \cdot \frac{T_n(t)}{T_{n,50\%} + T_n(t)}, \quad \text{(A3)}$$

where $g_{n,max}$ are the maximum conductances associated with total excitatory and inhibitory synapses. The parameters $T_{n,50\%}$ are the values of the variables $T_n(t)$ when $g_n(t)$ reach 50% of $g_{n,max}$.

Finally, we approximate the filtered membrane potential to its steady state:

$$V_{mf}(t) = \frac{[g_{exc}(t)/g_L] \cdot E_{exc} + [g_{inh}(t)/g_L] \cdot E_{inh} + E_L}{[g_{exc}(t)/g_L] + [g_{inh}(t)/g_L] + 1}, \quad \text{(A4)}$$

where g_L is the leak conductance and E_L, E_{exc} and E_{inh} are the leak, excitatory and inhibitory reversal potentials, respectively. Thus, Eqn A4 provides an approximate expression for the evolution of a filtered membrane potential, and the firing rate can be calculated using Eqn 5.

In summary, the model variables were calculated in the following steps. From the angular size $\theta(t-\delta_e)$, the angular edge velocity $\psi=\theta'(t-\delta_e)/2$ and the latency δ_e (obtained from Eqn 4), we calculated the presynaptic signal $pre(t-\delta_e)$ using Eqn A1. Then, integrating Eqn A2 with the Euler method and using Eqn A3, we calculated the excitatory and inhibitory conductances. Finally, we obtained the

filtered membrane potential, V_{mf}, using Eqn A4 and the firing rate R using Eqn 5.

Parameter selection and model fit

Based on intracellular recording and considering the resting membrane potential E_l=0 mV, we assumed the following values: excitatory synaptic reversal potential E_{exc}=60 mV; inhibitory synaptic reversal potential E_{inh}=−3 mV; excitatory time constant τ_{exc}=10 ms; and inhibitory time constant τ_{inh}=100 ms. Other parameters obtained from experimental measurements were: the firing rate exponent a_r=1, the rate baseline R_0=7 Hz and the rate slope k_r=7.7 Hz (Eqn 5). The constant ψ_{max} is selected to obtain an adimensional and normalized function f_{LMC}. For this purpose, its value was fixed as the maximum angular velocity for all stimuli, ψ_{max}=382 deg s^{-1}. The constant ψ_{min} was selected as 0.5 deg s^{-1}. The constant a_{LMC} is fitted by least squares. The signal $pre(t)$ was normalized to the highest response level obtained with stimulus 1 (which is the highest value attained for all stimuli). To satisfy this specification, the constant k_{pre} should be 0.0024 deg^{-2}. Parameters that could not be estimated using experimental information were approximated by nonlinear square error minimization between the average firing frequency and model prediction. We used all the stimuli to fit the experimental measurements, and the free parameters were optimized by least squares. The values obtained for the estimated parameters were: $(g_{exc,max}/g_L)$=25, $(g_{inh,max}/g_L)$ =107, $T_{exc,50\%}$=0.07, $T_{inh,50\%}$=0.02 and a_{LMC}=0.4. Note that, because the highest normalized excitatory and inhibitory conductances were related to the leak conductance, they are dimensionless (see Eqn A5). In addition, the parameters $T_{exc,50\%}$ and $T_{inh,50\%}$ are also dimensionless because they have identical units to the $pre(t)$ signal (see Eqn A2), which was normalized by its highest value for all stimuli.

With the optimization of these parameters only, a satisfactory fit can be achieved throughout all dynamics of expansion, including the initial phasic responses (Fig. 5C).

Competing interests

The authors declare no competing or financial interests.

Author contributions

D.E.O. and D.T., conception and design of research; D.E.O. performed experiments; D.E.O. analyzed data; D.E.O. and D.T. interpreted results of experiments; D.E.O. prepared figures; D.E.O. and D.T. drafted manuscript; D.E.O. and D.T. edited and revised manuscript; D.E.O. and D.T. approved final version of manuscript.

Funding

This work was supported by the Agencia Nacional de Promocion Cientifica y Tecnologica Argentina (ANPCYT) [grant nos. PICT 2012-2765 to D.O. and PICT 2013-0450 to D.T.] and the Universidad de Buenos Aires [grant no. 20020130100583BA to D.T.].

Supplementary information

Supplementary information available online at
http://jeb.biologists.org/lookup/doi/10.1242/jeb.136820.supplemental

References

Berón de Astrada, M. and Tomsic, D. (2002). Physiology and morphology of visual movement detector neurons in a crab (Decapoda: Brachyura). *J. Comp. Physiol. A* **188**, 539-551.
Berón de Astrada, M., Medan, V. and Tomsic, D. (2011). How visual space maps in the optic neuropils of a crab. *J. Comp. Neurol.* **519**, 1631-1639.
Berón de Astrada, M., Bengochea, M., Medan, V. and Tomsic, D. (2012). Regionalization in the eye of the grapsid crab *Neohelice granulata* (=*Chasmagnathus granulatus*): variation of resolution and facet diameters. *J. Comp. Physiol. A.* **198**, 173-180.
Borst, A. (1991). Fly visual interneurons responsive to image expansion. *Zool. Jb. Physiol.* **95**, 305-313.
Borst, A. and Bahde, S. (1988). Visual information processing in the fly's landing system. *J. Comp. Physiol. A.* **163**, 167-173.
Card, G. and Dickinson, M. (2008). Visually mediated motor planning in the escape response of *Drosophila*. *Curr. Biol.* **18**, 1300-1307.
Destexhe, A., Mainen, Z. F. and Sejnowski, T. J. (1994). An efficient method for computing synaptic conductances based on a kinetic model of receptor binding. *Neural. Comput.* **6**, 14-18.
Dunn, T. W., Gebhardt, C., Naumann, E. A., Riegler, C., Ahrens, M. B., Engert, F. and Del Bene, F. (2016). Neural circuits underlying visually evoked escapes in larval zebrafish. *Neuron* **89**, 613-628.
Fotowat, H. and Gabbiani, F. (2007). Relationship between the phases of sensory and motor activity during a looming-evoked multistage escape behavior. *J. Neurosci.* **27**, 10047-10059.
Fotowat, H. and Gabbiani, F. (2011). Collision detection as a model for sensory-motor integration. *Annu. Rev. Neurosci.* **34**, 1-19.
Fotowat, H., Fayyazuddin, A., Bellen, H. J. and Gabbiani, F. (2009). A novel neuronal pathway for visually guided escape in Drosophila melanogaster. *J. Neurophysiol.* **102**, 875-885.
Fotowat, H., Harrison, R. and Gabbiani, F. (2011). Multiplexing of motor information in the discharge of a collision detecting neuron during escape behaviors. *Neuron* **69**, 147-158.
Gabbiani, F., Krapp, H. G. and Laurent, G. (1999). Computation of object approach by a wide field, motion-sensitive neuron. *J. Neurosci.* **19**, 1122-1141.
Gabbiani, F., Krapp, H. G., Koch, C. and Laurent, G. (2002). Multiplicative computation in a visual neuron sensitive to looming. *Nature* **420**, 320-324.
Glantz, R. M. (1974). Defense reflex and motion detector responsiveness to approaching targets: the motion detector trigger to the defense reflex pathway. *J. Comp. Physiol.* **95**, 297-314.
Gray, J. R., Blincow, E. and Robertson, R. M. (2010). A pair of motion-sensitive neurons in the locust encode approaches of a looming object. *J. Comp. Physiol. A.* **196**, 927-938.
Hemmi, J. M. and Tomsic, D. (2012). The neuroethology of escape in crabs: from sensory ecology to neurons and back. *Curr. Opin. Neurobiol.* **22**, 194-200.
Herberholz, J. and Marquart, G. D. (2012). Decision making and behavioral choice during predator avoidance. *Front. Neurosci.* **6**, 1-15.
Jones, P. W. and Gabbiani, F. (2010). Synchronized neural input shapes stimulus selectivity in a collision-detecting neuron. *Curr. Biol.* **20**, 2052-2057.
Jones, P. W. and Gabbiani, F. (2012). Logarithmic compression of sensory signals within the dendritic tree of a collision-sensitive neuron. *J. Neurosci.* **32**, 4923-4934.
Land, M. and Layne, J. E. (1995). The visual control of behaviour in fiddler crabs. II. Tracking control systems in courtship and defence. *J. Comp. Physiol. A.* **177**, 91-103.
Layne, J., Wicklein, M., Dodge, F. A. and Barlow, R. B. (1997). Prediction of maximum allowable retinal slip speed in the fiddler crab, *Uca pugilator*. *Biol. Bull.* **193**, 202-203.
Maier, J. X., Neuhoff, J. G., Logothetis, N. K. and Ghazanfar, A. A. (2004). Multisensory integration of looming signals by rhesus monkeys. *Neuron* **43**, 177-181.
Medan, V., Oliva, D. and Tomsic, D. (2007). Characterization of lobula giant neurons responsive to visual stimuli that elicit escape behaviors in the crab *Chasmagnathus*. *J. Neurophysiol.* **98**, 2414-2428.
Medan, V., Beron de Astrada, M., Scarano, F. and Tomsic, D. (2015). A network of visual motion-sensitive neurons for computing object position in an arthropod. *J. Neurosci.* **35**, 6654-6666.
Oliva, D. (2015). Collision avoidance models, visually guided. In *Encyclopedia of Computational Neuroscience* (ed. D. Jaeger and R. Jung), pp. 626-645. Berlin: Springer-Verlag.
Oliva, D. and Tomsic, D. (2012). Visuo-motor transformations involved in the escape response to looming stimuli in the crab *Neohelice* (=*Chasmagnathus*) *granulata*. *J. Exp. Biol.* **215**, 3488-3500.
Oliva, D. and Tomsic, D. (2014). Computation of object approach by a system of visual motion-sensitive neurons in the crab Neohelice. *J. Neurophysiol.* **112**, 1477-1490.
Oliva, D., Medan, V. and Tomsic, D. (2007). Escape behavior and neuronal responses to looming stimuli in the crab *Chasmagnathus granulatus* (Decapoda: Grapsidae). *J. Exp. Biol.* **210**, 865-880.
Peron, S. P. and Gabbiani, F. (2009). Spike frequency adaptation mediates looming stimulus selectivity in a collision-detecting neuron. *Nat. Neurosci.* **12**, 318-326.
Preuss, T., Osei-Bonsu, P. E., Weiss, S. A., Wang, C. and Faber, D. S. (2006). Neural representation of object approach in a decision-making motor circuit. *J. Neurosci.* **26**, 3454-3464.
Rind, F. C. (1996). Intracellular characterization of neurons in the locust brain signaling impending collision. *J. Neurophysiol.* **75**, 986-995.
Rind, F. C. and Bramwell, D. I. (1996). Neural network based on the input organization of an identified neuron signaling impending collision. *J. Neurophysiol.* **75**, 967-985.
Rind, F. C. and Simmons, P. J. (1992). Orthopteran DCMD neuron: a reevaluation of responses to moving objects. I. Selective responses to approaching objects. *J. Neurophysiol.* **68**, 1654-1666.

Santer, R. D., Yamawaki, Y., Rind, F. C. and Simmons, P. J. (2005). Motor activity and trajectory control during escape jumping in the locust *Locusta migratoria*. *J. Comp. Physiol. A.* **191**, 965-975.
Santer, R. D., Yamawaki, Y., Rind, F. C. and Simmons, P. J. (2008). Preparing for escape: an examination of the role of the DCMD neuron in locust escape jumps. *J. Comp. Physiol. A* **194**, 69-77.
Silva, A. C., McMillan, G. A., Santos, C. P. and Gray, J. R. (2015). Background complexity affects response of a looming-sensitive neuron to object motion. *J. Neurophysiol.* **113**, 218-231.
Simmons, P. J., Rind, F. C. and Santer, R. D. (2010). Escapes with and without preparation: the neuroethology of visual startle in locusts. *J. Insect Physiol.* **56**, 876-883.
Srinivasan, M. V. and Zhang, S. (2004). Visual motor computations in insects. *Annu. Rev. Neurosci.* **27**, 679-696.
Sun, H. and Frost, B. J. F. (1998). Computation of different optical variables of looming objects in pigeon nucleus rotundus neurons. *Nat. Neurosci.* **1**, 296-303.
Sztarker, J. and Rind, F. C. (2014). A look into the cockpit of the developing locust: looming detectors and predator avoidance. *Dev. Neurobiol.* **74**, 1078-1095.
Sztarker, J., Strausfeld, N. J. and Tomsic, D. (2005). Organization of optic lobes that support motion detection in a semiterrestrial crab. *J. Comp. Neurol.* **493**, 396-411.
Tammero, L. F. and Dickinson, M. H. (2002). Collision-avoidance and landing responses are mediated by separate pathways in the fruit fly, *Drosophila melanogaster*. *J. Exp. Biol.* **205**, 2785-2798.
Wagner, H. (1982). Flow-field variables trigger landing in flies. *Nature* **297**, 147-148.
Wang, Y. and Frost, B. J. (1992). Time to collision is signalled by neurons in the nucleus rotundus of pigeons. *Nature* **356**, 236-238.
Wasserman, L. (2004). *All of Statistics. A Concise Course in Statistical Inference*, Chapter 8, pp. 107-116. New York: Springer.